Available online at www.sciencedirect.com
ScienceDirect
Trans. Nonferrous Met. Soc. China 32(2022) 3212−3221
Transactions of Nonferrous Metals Society of China
www.tnmsc.cn

Grain refinement of Mg−Al binary alloys inoculated by in-situ oxidation

Heng-bin LIAO[1*], Li-ling MO[1*], Cheng-bo LI[1,2], Mei-yan ZHAN[1], Jun DU[1]

1. School of Materials Science and Engineering, South China University of Technology, Guangzhou 510640, China;
2. School of Materials and Environment, Guangxi University for Nationalities, Nanning 530006, China

Received 30 August 2021; accepted 30 December 2021

Abstract: Utilizing oxide inclusion to induce heterogeneous nucleation event is an available method to achieve grain refinement. In this study, Mg−Al binary alloys were refined by inoculation of in-situ oxidation process. Results show that MgO and $MgAl_2O_4$ phases are primary oxide products for Mg−*x*Al alloys inoculated by in-situ oxidation. For pure Mg and Mg−1Al alloy, MgO is the only oxide product. $MgAl_2O_4$ is another oxide product for Mg−*x*Al alloy as Al content increases to 3 wt.%. For Mg−3Al alloy, average grain size significantly decreases from 1135 to 237 μm, with a high grain refining ratio of 79.1%. Both MgO and $MgAl_2O_4$ possess nucleating potency for α-Mg grain. $MgAl_2O_4$ exhibits a higher nucleating potency due to the lower misfit with α-Mg. The grain refinement of Mg−*x*Al alloys inoculated by in-situ oxidation process is attributed to heterogeneous nucleation events of α-Mg grains on MgO or $MgAl_2O_4$ particles.

Key words: Mg−Al alloy; grain refinement; heterogeneous nucleation; MgO; $MgAl_2O_4$

1 Introduction

Due to the low density and high specific strength, Mg alloys are considered to be the promising lightest structural materials and have been applied in automobile, aerospace, 3C electronic products and other fields [1−4]. Despite significant weight saving potential, Mg alloys account for only a small part of the products in relevant fields [5]. The relatively low tensile strength and poor deformation capacity limit their wider application. Usually, grain refinement is good for enhancing mechanical properties of metallic materials [6,7]. Fine microstructure is also desirable for reduction of casting defects and will benefit the subsequent processing of plastic deformation. Promoting heterogeneous nucleation is a common industrial method to achieve grain refinement [8].

Among all Mg alloys, Mg−Al series alloys such as AM60 and AZ91 play a dominant role in the Mg alloy products [9−12]. Carbon inoculation is a very effective grain refining method for Al-bearing Mg alloys [9,13,14]. It has been widely recognized that Al_4C_3 particle acts as an available nucleating site for α-Mg grain. Al element is indispensable for carbon inoculated Mg alloys. Actually, Al element also plays an important role in the heterogeneous nucleation events of Mg−RE series alloys [15−18]. The addition of Al element resulted in an obvious decrease in grain size of Mg−6Sm from 1830 to 30 μm [16]. The in-situ formed Al_2Sm particle exhibited an orientation relationship (OR) with Mg matrix and was regarded as the nucleating site. Meanwhile, Al_2RE series particles such as Al_2Y, Al_2Ce or Al_2Nd were predicted to be the effective nucleating substrates of α-Mg grain [17]. For Mg−RE alloys, Al element

*Heng-bin LIAO and Li-ling MO contributed equally to this work

Corresponding author: Jun DU, Tel/Fax: +86-20-87113597, E-mail: tandujun@sina.com

DOI: 10.1016/S1003-6326(22)66014-X

might be a promising substitution of Zr.

In the past two decades, oxide inoculation has been proved as a significant method to refine Mg and its alloys [9,19−26]. Despite the fact that oxide inclusions are the common impurities to deteriorate mechanical properties, they were found to be in favor of grain refinement of α-Mg grain. FAN et al [21,25] found that AZ91 alloy can be significantly refined via intensive shearing treatment. The MgO particles derived from oxide film exhibited a crystallographic OR with α-Mg matrix and were considered as nucleating sites for α-Mg grain. After intensive shearing treatment, the high pressure die casting AZ91 alloy exhibited a higher ultimate tensile strength and elongation [24]. Moreover, CaO and ZnO were also considered as the available nucleating substrates for α-Mg grains due to the low misfit between CaO or ZnO and α-Mg [22,23,27]. MA et al [20] found that the addition of MgO powder can effectively refine Mg−3Al alloy with an average grain size decreasing from 535 to 112 μm. They considered that MgO would react with Al to form $MgAl_2O_4$ which may be the heterogeneous nucleating sites for α-Mg grains. It was also reported that $MgAl_2O_4$ particles were in-situ formed and induced the heterogeneous nucleation by introducing O_2 or some unstable oxides in Al−Mg melt [28−30]. In our previous work, the addition of $MgAl_2O_4$ powder resulted in grain refinement of Mg−Al alloy [19]. $MgAl_2O_4$ possessing a small misfit with α-Mg is considered as an available nucleating substrate for α-Mg grain. MgO and $MgAl_2O_4$ are common oxide products for Al-bearing Mg alloy during at high temperatures especially in heating and smelting [31−33].

It is difficult to completely avoid the oxide inclusions in Mg melt even under the protective gas. Due to the nucleating capability of oxide, it may be available to utilize such oxide inclusions for grain refinement of Mg alloy. This is similar to the oxide metallurgy technology of steel [34,35]. Hence, the in-situ oxidation processes (in-situ OP) were proposed to refine Mg grains of AZ31 alloy [36]. In this study, Mg−Al binary alloys were chosen and inoculated by in-situ OP. We aim to clarify the grain refinement mechanism of Mg−Al binary alloys inoculated by in-situ OP and whether Al element affects the grain refining effect and heterogeneous nucleation events.

2 Experimental

In this study, Mg−xAl (x=0, 1, 3 and 6 wt.%) alloys were prepared from pure Mg (99.95 wt.%, Shanxi Regal Advanced Materials Co., Ltd., China) and high purity Al (99.99 wt.%, Zhongnuo Advanced Material (Beijing) Technology Co., Ltd., China). Firstly, pure Mg ingot was placed in an MgO crucible and melted to 760 °C in an electric resistance furnace under the protective atmosphere (99.5 vol.% N_2 and 0.5 vol.% SF_6). After that, high purity Al was added into the Mg melt. After being held for 10 min, the Mg−Al melt was treated by the in-situ oxidation process, i.e. simultaneously by introducing a mixed gas of O_2 and Ar with the gas flow rates of 10 and 100 mL/min for 10 min, respectively, and stirring manually [36]. After treatment, a salt flux composed of NaCl, KCl, $MgCl_2$ and CaF_2 with mass fractions of 10%, 35%, 45% and 10%, respectively, was used to cover Mg−Al melt. The crucible containing the inoculated melt was placed in air at room temperature until the melt returned to the preset value of 760 °C. Then, they were taken into the electric resistance furnace and kept for 10 min. Finally, the melt was poured into a cylindrical mild steel mold (d40 mm × 60 mm, as shown in Fig. 1) pre-heated at 500 °C.

The specimens for observing the grain morphology were sectioned at 20 mm from the bottom of casting ingots and heat-treated at 420 °C for 8 h and then cooled down to room temperature in the air. After being ground and polished, the specimens were etched by using a 5 vol.% nitric alcohol solution. The grain morphologies were observed by using an optical camera and used to measure average grain sizes via a linear intercept method as per ASTM E112—88. Grain refining ratio (δ) is obtained by Eq. (1):

$$\delta=\frac{d_1-d_2}{d_1} \tag{1}$$

where d_1 is the average grain size before inoculation, and d_2 is the average grain size after inoculation.

The detailed characteristics of the microstructures of as-cast samples were investigated via a scanning electron microscope (SEM, Quanta 200) equipped with an energy-dispersive spectroscope (EDS), and a transition electron microscope (TEM, JEOL 2100F, operated at 200 kV). The TEM

samples were obtained via focused ion beam (FIB, FEI Scios) technique. A thin slice of oxide inclusions boned with a part of Mg matrix was cut and then milled by medium current (100−3000 pA) and polished by small current (16−48 pA) to electron transparency, using a Ga^+ ion beam source.

3 Results and discussion

3.1 Grain refinement of Mg−*x*Al alloys inoculated by in-situ OP

Figure 2 shows the grain morphologies of Mg−*x*Al alloys without and with inoculation of in-situ OP. It is clear in Fig. 2 that all Mg−*x*Al alloys are effectively refined after inoculation by in-situ OP. Figure 3 shows the average grain sizes and grain refining ratios. For Mg−*x*Al alloys without inoculation, grain morphology exhibits a transition from a coarse columnar crystal to a fine fully equiaxed crystal with the increase in Al content, which is due to the growth restricting effect. After inoculation, pure Mg changes from coarse columnar structure to fine columnar structure with an average grain size decreasing from 5708 to 1800 μm. Average grain sizes of Mg−1Al, Mg−3Al and Mg−6Al alloys decrease from 2600, 1135 and 433 μm to 1458, 237 and 172 μm, respectively. Accordingly, grain refining ratios for pure Mg, Mg−1Al, Mg−3Al and Mg−6Al alloys inoculated by in-situ OP are 0.685, 0.439, 0.791 and 0.603, respectively.

3.2 Observation of oxide inclusions

Figure 4 shows the typical SEM micrographs and EDS results for pure Mg and Mg−3Al alloy without and with inoculation of in-situ OP. Pure Mg exhibits a single-phase structure of α-Mg matrix, as shown in Fig. 4(a). Mg melt has strong oxygen

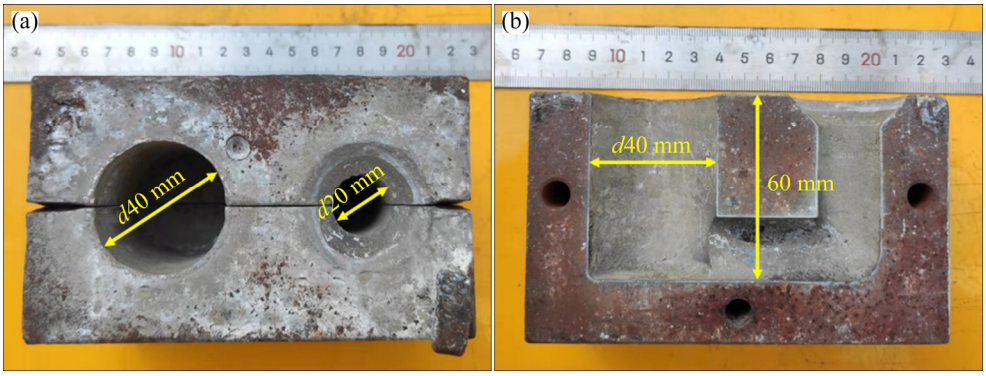

Fig. 1 Casting mold (a) and cross-section of casting mold (b)

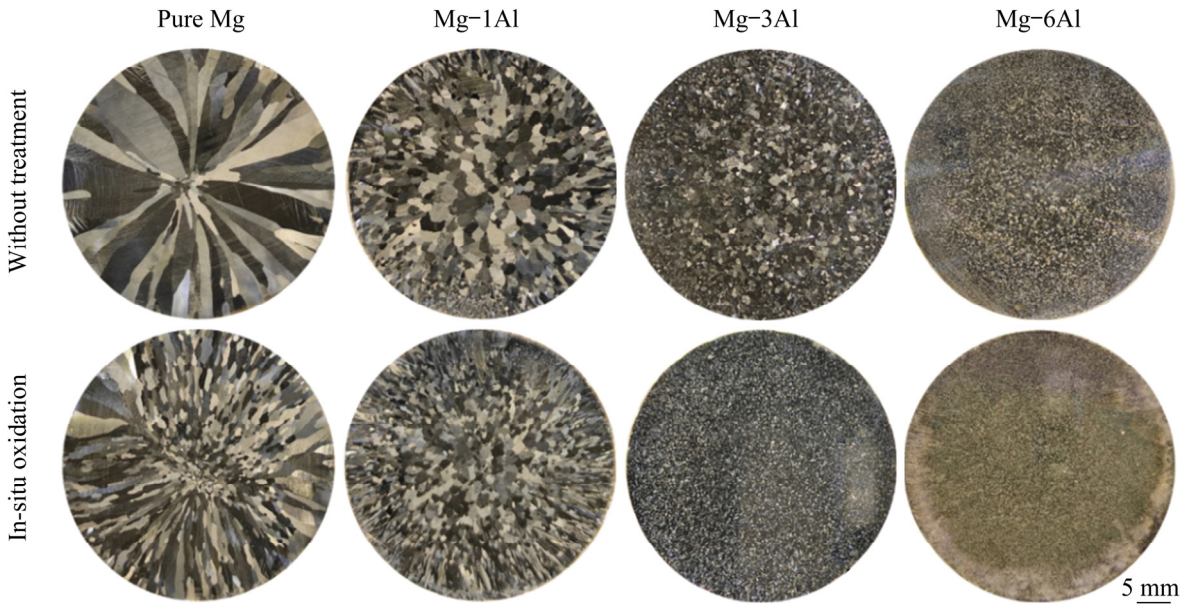

Fig. 2 Grain morphologies of Mg−*x*Al (*x*=0, 1, 3 and 6 wt.%) alloys without and with inoculation of in-situ OP

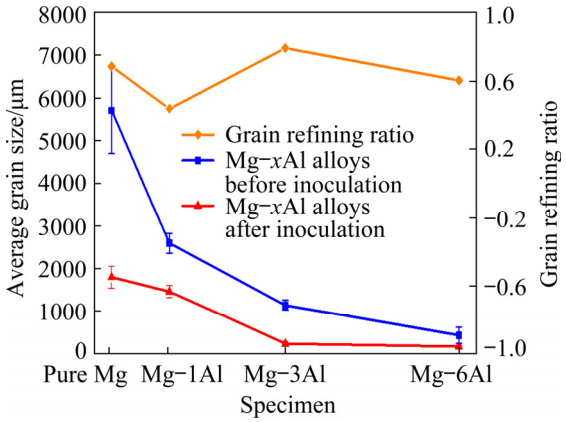

Fig. 3 Average grain sizes of Mg−*x*Al alloys without and with inoculation of in-situ OP, and grain refining ratios

affinity and will react with oxygen when introducing a mixed gas of O_2 and Ar. After inoculation, MgO is in-situ generated with a size of 1−3 μm, as shown in Figs. 4(b, c). From Fig. 4(e), Mg−3Al alloy mainly consists of Mg matrix and $Mg_{17}Al_{12}$ phase. The $Mg_{17}Al_{12}$ phase shows a discontinuous distribution due to the non-equilibrium solidification. After inoculation of in-situ OP, oxide particles are also introduced in Mg−3Al alloy, as shown in Figs. 4(f−h). According to the EDS results in Fig. 4, some oxide particles have a higher Al content than Mg matrix. Meanwhile, it is found that an Al-rich Mg—O particle has Al/O molar ratio closing to 1:2, meeting the stoichiometric ratio of $MgAl_2O_4$ spinel, as shown in Figs. 4(h, l). The $MgAl_2O_4$ spinel was also found in the oxidation products of Al-bearing Mg alloys [31−33].

Figures 5 and 6 show the bright-field images and selected-area electronic diffraction (SAED) patterns of the in-situ OP inoculated Mg−3Al alloy. According to the SAED patterns, the second phases of Regions 1 and 2 are identified as $MgAl_2O_4$ phase. The MgO phase is also detected by TEM, as shown in Fig. 6. It can be seen that MgO and $MgAl_2O_4$ are the primary oxide inclusions of Mg−3Al alloys after inoculation of in-situ OP.

To further investigate the types of oxide inclusions in the inoculated Mg−*x*Al alloys, contents (molar fraction) of Al and O elements of oxide inclusion particles are determined, as shown in Fig. 7. There is no doubt that MgO is the only oxide in inoculated pure Mg. For inoculated Mg−1Al, MgO particles are also mainly oxide inclusions. Despite a few Mg—O particles containing low Al

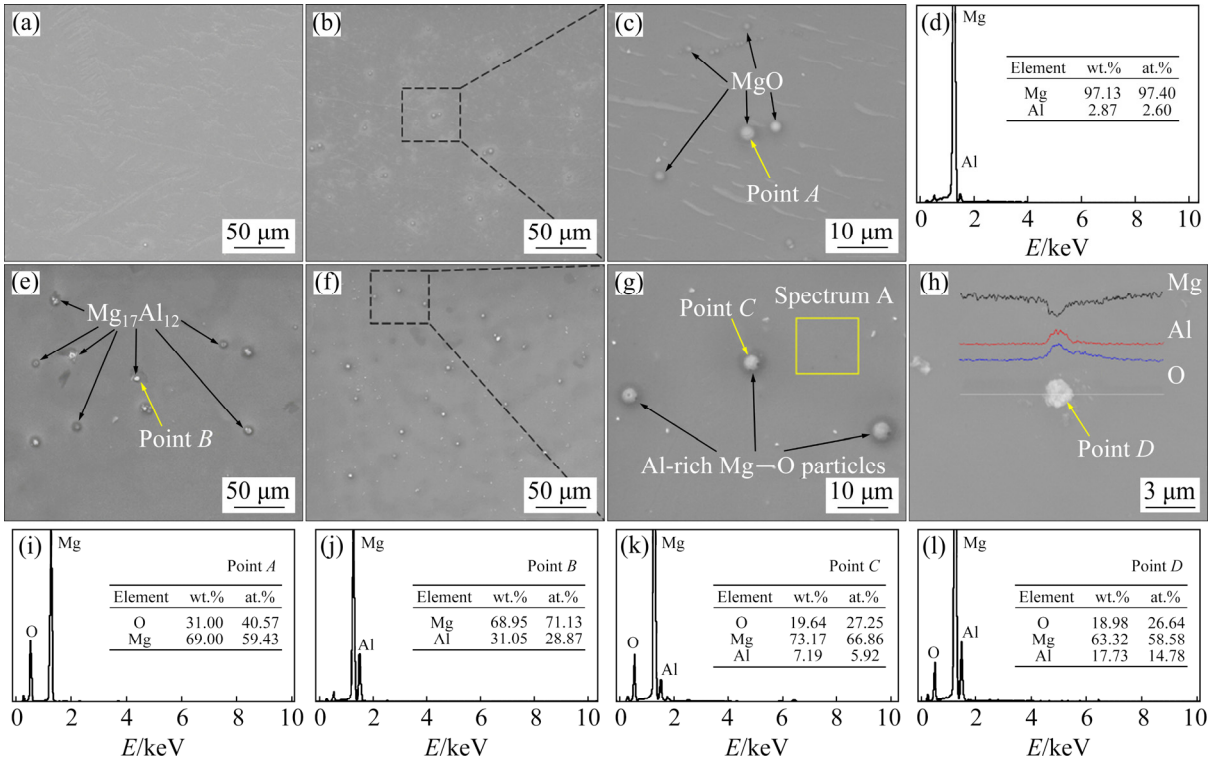

Fig. 4 Typical SEM micrographs (a−c, e−h) and EDS results (d, i−l) of pure Mg (a), inoculated pure Mg (b, c), Mg−3Al (e) and inoculated Mg−3Al (f−h)

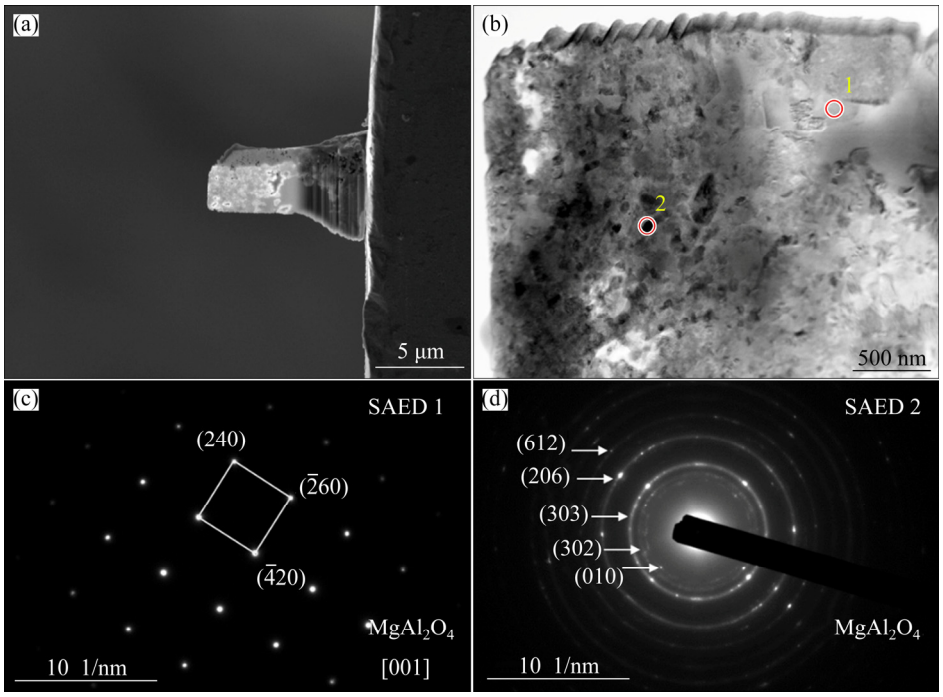

Fig. 5 TEM image of oxide inclusions boned with part of Mg matrix in Mg−3Al alloy with inoculation of in-situ OP (a), bright-field image (b) and SAED patterns (c, d) of Regions 1 and 2 in (b), respectively

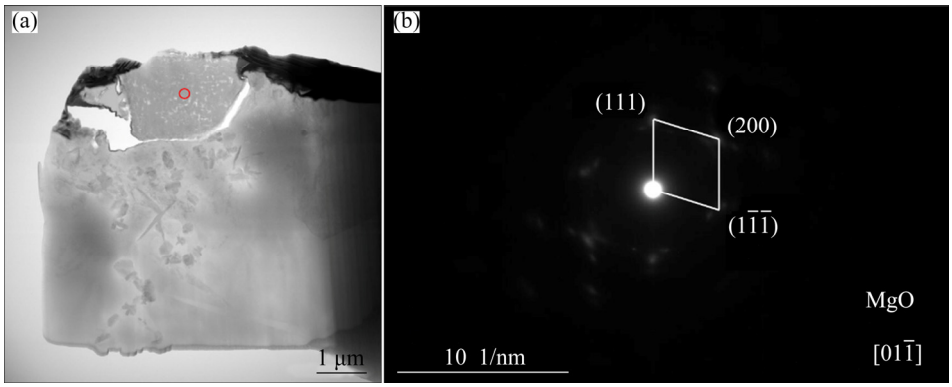

Fig. 6 Bright-field image of inoculated Mg−3Al alloy (a) and SAED pattern (b) in (a)

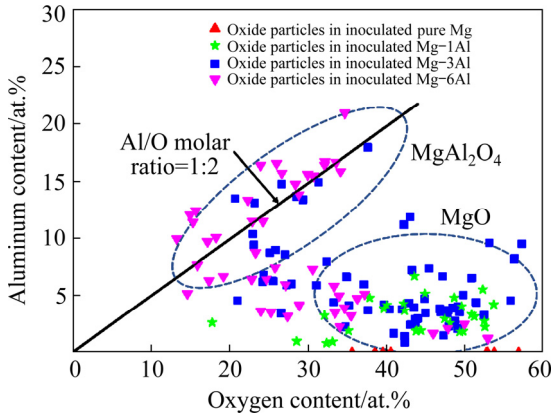

Fig. 7 Contents of Al and O elements of oxide inclusion particles in pure Mg and Mg−*x*Al alloys inoculated by in-situ OP

content (<5 at.%), the O element is higher than 40 at.%. Hence, they are classified as MgO particles. In the inoculated Mg−3Al alloy, Mg—O particles with a high content of O element and low content of Al element are also deemed to MgO particles. While partial Al-rich Mg—O particles exhibit an molar ratio of Al to O close to 1:2, thereby being seen as $MgAl_2O_4$ particles, which is corresponding to the TEM results in Fig. 5. Similarly, MgO and $MgAl_2O_4$ are observable oxide inclusions in the inoculated Mg−6Al alloy. Meanwhile, the amount of $MgAl_2O_4$ particles in the inoculated Mg−6Al alloy is higher than that of inoculated Mg−3Al alloy, as shown in elliptic region in Fig. 7.

3.3 Grain refinement mechanism of Mg−*x*Al alloys inoculated by in-situ OP

Owing to the lack of solute segregation restricting grain growth, α-Mg grain of inoculated pure Mg still exhibits the morphology of columnar crystal even if pure Mg is availably refined. The MgO particle as the only second phase is deemed to be nucleating substrate for α-Mg grain. Table 1 shows the misfits between α-Mg and MgO or $MgAl_2O_4$ by experiment or calculation based on the edge-to-edge matching (E2EM) model. Due to the suitable crystallographic misfit (with an f_r of 7.63% and an f_d of 1.18%; f_r is the atomic spacing misfit of matching directions and f_d is the d-value mismatch of matching planes) between α-Mg and MgO, MgO has the potential nucleating potency for α-Mg. The ORs were experimentally detected as $\langle 1\bar{2}10\rangle\{0002\}_{Mg}//\langle 01\bar{1}\rangle\{111\}_{MgO}$ with an atomic misfit of 5.46% in the MgO inoculated AZ91D alloy, and $[01\bar{1}1]_{Mg}//[0\bar{1}1]_{MgO}$ in $(0\bar{1}12)_{Mg}//(200)_{MgO}$ with an atomic misfit of 3.2% [21,25]. Meanwhile, the first-principles calculation results showed that the interfacial bond strength between Mg and MgO is higher than that of Mg−Mg, suggesting that Mg atoms can epitaxially grow on the MgO $(1\bar{1}1)$ surface [37]. The geometrical feature like the sizes of nucleating particle will affect the heterogeneous nucleation events. Usually, size of effective particles may range from 1 to a few microns [38]. In this study, in-situ formed MgO particles with a size of 1−3 μm would meet the demand of effective heterogeneous nucleation event.

Table 1 Misfit obtained by experiments or calculation (E2EM model) between α-Mg and MgO or $MgAl_2O_4$

Matching or orientation relationship	Misfit/%		Source
	f_r	f_d	
$\langle 11\bar{2}0\rangle_{Mg}//\langle 110\rangle_{MgO}$ in $\{10\bar{1}1\}_{Mg}//\{111\}_{MgO}$	7.63	1.18	This work
$\langle 1\bar{2}10\rangle_{Mg}//\langle 01\bar{1}\rangle_{MgO}$ in $\{0002\}_{Mg}//\{111\}_{MgO}$	5.46	–	[25]
$[01\bar{1}1]_{Mg}//[0\bar{1}1]_{MgO}$ in $(0\bar{1}12)_{Mg}//(200)_{MgO}$	3.2	–	[21]
$\langle 10\bar{1}0\rangle_{Mg}//\langle 110\rangle_{MgAl_2O_4}$ in $\{0002\}_{Mg}//\{1\bar{1}3\}_{MgAl_2O_4}$	2.34	5.53	[19]
$\langle 11\bar{2}3\rangle_{Mg}//\langle 110\rangle_{MgAl_2O_4}$ in $\{10\bar{1}1\}_{Mg}//\{1\bar{1}3\}_{MgAl_2O_4}$	7.49	1.03	[19]

When Mg−Al melts are treated by in-situ OP, O_2 will quickly reach equilibrium and react with Mg and Al atoms. Based on the available thermodynamic data [39], the potential oxidizing reactions in the inoculated Mg−Al melt are as follows:

$$2Al(l)+3/2O_2(g)=Al_2O_3(s),\quad \Delta G^{\Theta}_{1033\ K}=-1279\ kJ/mol \tag{2}$$

$$2Mg(l)+O_2(g)=2MgO(s),\quad \Delta G^{\Theta}_{1033\ K}=-848\ kJ/mol \tag{3}$$

$$Al_2O_3(s)+MgO(s)=MgAl_2O_4(s),\quad \Delta G^{\Theta}_{1033\ K}=-47\ kJ/mol \tag{4}$$

$$Mg(l)+2Al(l)+2O_2(g)=MgAl_2O_4(s),\quad \Delta G^{\Theta}_{1033\ K}=-1889\ kJ/mol \tag{5}$$

Figure 8 shows the Gibbs free energy change of potential oxidizing reactions as a function of Al content in the inoculated Mg−Al melts at 1033 K, which are based on the van't Hoff equation and "sub-regular" solution models. It seems that Al_2O_3, MgO and $MgAl_2O_4$ are the thermodynamically potential oxidizing products in the inoculated Mg−Al melts, while Al_2O_3 is not detected in the present results. According to the Ellingham diagram, Mg has a higher affinity with oxygen than Al [40]. Hence, Al_2O_3 may not be generated in the Mg−*x*Al melt with in-situ OP or react with Mg melt to form MgO and Al solute. The formation of $MgAl_2O_4$ would also consume Al_2O_3 by Reaction (4). It is seen that MgO and $MgAl_2O_4$ might be the primary oxide inclusions in the Mg−Al melt inoculated by in-situ OP, which is in accordance with the observation of oxide inclusions by SEM and TEM.

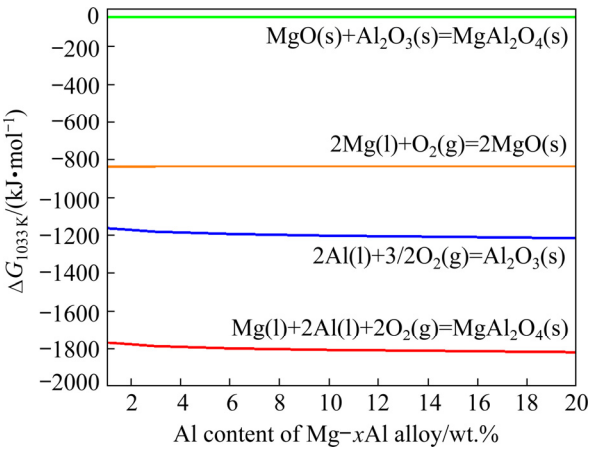

Fig. 8 Gibbs free energy change of potential oxidizing reactions as function of Al content in inoculated Mg−*x*Al melts at 1033 K

From the statistics of elementary composition of oxide inclusions, MgO particle might be primary oxide for Mg−1Al alloy inoculated by in-situ OP. Despite the fact that formation of $MgAl_2O_4$ is thermodynamically feasible, there is no observation of $MgAl_2O_4$ particles in the inoculated Mg−1Al alloy. It is confirmed from Fig. 7 that both MgO and $MgAl_2O_4$ particles are primary oxidation products in the inoculated Mg−3Al alloy. It is also believed from SEM and TEM results that $MgAl_2O_4$ would be the important oxide inclusion for the inoculated Mg−3Al alloy. Similar to the inoculated Mg−3Al, MgO and $MgAl_2O_4$ oxide inclusions are also easily detected in the inoculated Mg−6Al alloy. Judging from the statistics of oxide inclusions, the amount of $MgAl_2O_4$ in Mg−6Al is higher than that of Mg−3Al with inoculation. Al content would affect the formation of $MgAl_2O_4$ in the inoculated Mg−Al melt.

For sustaining the stable existence of pure $MgAl_2O_4$ phase in the Mg−Al system with oxygen, the chemical potential $\Delta\mu_i$ should be satisfied with the following constraints:

$$\Delta\mu_{Mg}\leq 0,\ \Delta\mu_{Al}\leq 0,\ \Delta\mu_{O}\leq 0 \tag{6}$$

$$\Delta\mu_{Mg}+2\Delta\mu_{Al}+4\Delta\mu_{O}=\Delta H_{f,MgAl_2O_4} \tag{7}$$

$$\Delta\mu_{Mg}+\Delta\mu_{O}\leq\Delta H_{f,MgO} \tag{8}$$

$$2\Delta\mu_{Al}+3\Delta\mu_{O}\leq\Delta H_{f,Al_2O_3} \tag{9}$$

where ΔH_f is the formation enthalpy.

Figure 9 shows the thermodynamic stable ranges of chemical potential region for equilibrium growth of oxide in Mg−Al−O system. The calculated chemical potential regions of Mg, Al and O are based on the first-principles calculations by density functional theory (DFT). Herein, $MgAl_2O_4$ can be stably formed in the narrow area of *DEFG*. At the Mg-rich corner, MgO is the primary oxide. With the Al chemical potential ($\Delta\mu_{Al}$) increasing, $MgAl_2O_4$ would be another phase for Mg−Al−O system. Thus, with the Al content increasing, $MgAl_2O_4$ is inclined to form in Mg−Al melts inoculated by in-situ OP.

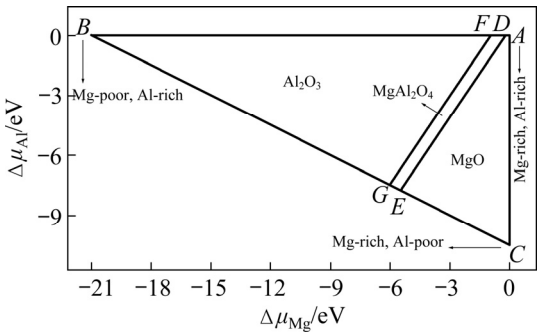

Fig. 9 Thermodynamic stable ranges of chemical potential region for equilibrium growth of oxide in Mg−Al−O system

$MgAl_2O_4$ exhibiting the heterogeneous nucleating potency for Mg−Al alloys has been confirmed in the previous work [19]. The addition of $MgAl_2O_4$ powder leads to a significant decrease in grain size of pure Mg and Mg−Al alloys [19,36]. The calculation based on E2EM model indicated that the matching relationships of $\langle 10\bar{1}0\rangle_{Mg}//\langle 110\rangle_{MgAl_2O_4}$ in $\{0002\}_{Mg}//\{1\bar{1}3\}_{MgAl_2O_4}$ with an f_r of 2.34% and $\langle 11\bar{2}3\rangle_{Mg}//\langle 110\rangle_{MgAl_2O_4}$ in $\{10\bar{1}1\}_{Mg}//\{1\bar{1}3\}_{MgAl_2O_4}$ with an f_r of 7.49% are the possible ORs for α-Mg and $MgAl_2O_4$, as shown in Table 1. Compared to MgO, the $MgAl_2O_4$ particles have a higher nucleating potency for α-Mg grain due to the lower misfit and nucleating undercooling. Thus, for Mg−1Al inoculated by in-situ OP, grain refinement should be attributed to the heterogeneous nucleation event of α-Mg grain on MgO particles. While for Mg−3Al and Mg−6Al alloys, due to the co-existence of MgO and $MgAl_2O_4$, significant grain refinement is due to the heterogeneous nucleation of α-Mg grain on MgO and $MgAl_2O_4$ particles.

According to the classical solidification theory, the final grain structure of metallic materials should be determined by the nucleation and growth condition during the solidification. Usually, grain will preferentially nucleate in the wall of casting mold and grow toward the center of the melt. Thus, pure Mg exhibits the coarse columnar structure. During Mg−Al melt solidification in the non-equilibrium, Al solute will be released from the nucleated grain and segregate in the front of the solid−liquid interface, restricting the growth of α-Mg grain of columnar morphology. Moreover, a constitutional undercooling is developed and promotes the nucleation events especially for the heterogeneous nucleation. The heterogeneous nucleation events can also be affected by the initial developing rate of constitutional undercooling, which is defined by

$$\frac{d\Delta T_c}{df_s}=m_1c_0\left(k-1\right) \tag{10}$$

where ΔT_c is the constitutional undercooling, f_s is

the volume fraction of the solid, m_l is the gradient of the liquidus slope, c_0 is the concentration of the solute in binary alloy, and k is the equilibrium partition coefficient. Note that growth restriction factor is also $m_l c_0(k-1)$, which is designated as Q [41]. Therefore, there is a transition from columnar structure to fully equiaxed grain structure when Al content of Mg−xAl alloys increases from 0 to 6 wt.%.

For pure Mg refined by in-situ OP, the grain size of α-Mg decreases with a grain refining ratio of 68.5%. Owing to an obvious growth restricting effect of Al in pure Mg, there is a significant decrease in grain size from 5708 to 2600 μm when 1 wt.% Al is added into pure Mg. Accordingly, there is lower grain refining ratio of 43.9% for Mg−1Al inoculated by in-situ OP. With Al content increasing to 3 wt.%, a higher refining ratio of 79.1% is obtained. The $MgAl_2O_4$ with a higher nucleating potency contributes to the high grain refining ratio due to the lower misfit. Meanwhile, constitutional undercooling induced by solute segregation will increase as the Al content increases from 1 wt.% to 3 wt.%. According to the interdependence theory [42], the lower nucleation undercooling of $MgAl_2O_4$ particles and the increase of constitutional undercooling are in favor of the high grain refining ratio. As Al content increases from 3 wt.% to 6 wt.%, an obvious decrease in grain size from 1135 to 433 μm is obtained. While there is a slight decrease from 237 to 172 μm for the inoculated Mg−Al alloy. Hence, there is a decrease from 79.1% to 60.3% in grain refining ratio for Mg−Al inoculated by in-situ OP when Al content increases from 3 wt.% to 6 wt.%.

4 Conclusions

(1) Grain refinement of Mg−xAl alloys is achieved by inoculation of in-situ OP. With inoculation, grain size of pure Mg decreases from 5708 to 1800 μm. The Mg−3Al alloy shows a high grain refining ratio of 79.1%, with an average grain size declining from 1135 to 237 μm.

(2) MgO particles are the only oxide inclusion for pure Mg and Mg−1Al alloy with inoculation of in-situ OP. In addition to MgO particle, $MgAl_2O_4$ is another oxide product in the inoculated Mg−3Al and Mg−6Al alloys. $MgAl_2O_4$ phase is inclined to form in the inoculated Mg−Al alloy when Al content increases to 3 wt.%.

(3) For pure Mg and Mg−1Al alloy inoculated by in-situ OP, grain refinement is attributed to the heterogeneous nucleation of α-Mg grain on MgO particles. While for Mg−3Al and Mg−6Al alloys, the grain refinement should be attributed to heterogeneous nucleation events on both $MgAl_2O_4$ and MgO. The $MgAl_2O_4$ exhibits a lower atomic misfit with α-Mg than MgO.

Acknowledgments

This work was supported by the National Natural Science Foundation of China (No. 51871100).

References

[1] WEILER J P. A review of magnesium die-castings for closure applications [J]. Journal of Magnesium and Alloys, 2019, 7: 297−304.

[2] POURBAHARI B, MIRZADEH H, EMAMY M. Elucidating the effect of intermetallic compounds on the behavior of Mg−Gd−Al−Zn magnesium alloys at elevated temperatures [J]. Journal of Materials Research, 2017, 32: 4186−4195.

[3] LIANG Xin-li, PENG Xiang, JI Hao, LIU Wen-cai, WU Guo-hua, DING Wen-jiang. Microstructure and mechanical properties of as-cast and solid solution treated Mg−8Li−xAl−yZn alloys [J]. Transactions of Nonferrous Metals Society of China, 2021, 31: 925−938.

[4] FU Peng-huai, WANG Nan-qian, LIAO Hai-guan, XU Wen-yu, PENG Li-ming, CHEN Juan, HU Guo-qi, DING Wen-jiang. Microstructure and mechanical properties of high strength Mg−15Gd−1Zn−0.4Zr alloy additive-manufactured by selective laser melting process [J]. Transactions of Nonferrous Metals Society of China, 2021, 31: 1969−1978.

[5] JOOST W J, KRAJEWSKI P E. Towards magnesium alloys for high-volume automotive applications [J]. Scripta Materialia, 2015, 128: 107−112.

[6] YU Hui-hui, XIN Yun-chang, WANG Mao-yin, LIU Qing. Hall−Petch relationship in Mg alloys: A review [J]. Journal of Materials Science & Technology, 2018, 34: 248−256.

[7] CHEN Xiang, HUANG Guang-sheng, LIU Shuai-shuai, HAN Ting-zhuang, JIANG Bin, TANG Ai-tao, ZHU Yun-tian, PAN Fu-sheng. Grain refinement and mechanical properties of pure aluminum processed by accumulative extrusion bonding [J]. Transactions of Nonferrous Metals Society of China, 2019, 29: 437−447.

[8] WANG Y, FANG C M, ZHOU L, HASHIMOTO T, ZHOU X, RAMASSE Q M, FAN Z. Mechanism for Zr poisoning of Al−Ti−B based grain refiners [J]. Acta Materialia, 2019, 164: 428−439.

[9] DU Jun, YAO Ze-jiang, HAN Shuai, LI Wen-fang. Discussion on grain refining mechanism of AM30 alloy inoculated by $MgCO_3$ [J]. Journal of Magnesium and Alloys, 2017, 5: 181−188.

[10] PAN Fu-sheng, YANG Ming-bo, CHEN Xian-hua. A review on casting magnesium alloys: Modification of commercial alloys and development of new alloys [J]. Journal of Materials Science & Technology, 2016, 32: 1211−1221.

[11] MEHRANPOUR M S, HEYDARINIA A, EMAMY M, MIRZADEH H, KOUSHKI A, RAZI R. Enhanced mechanical properties of AZ91 magnesium alloy by inoculation and hot deformation [J]. Materials Science and Engineering: A, 2021, 802: 140667.

[12] CAO Li-jie, MA Guo-rui, WANG Chun-xia, CHEN Zheng-jian, ZHANG Jia-heng. Effect of compression ratio on microstructure evolution of Mg−10%Al−1%Zn−1%Si alloy prepared by SIMA process [J]. Transactions of Nonferrous Metals Society of China, 2021, 31: 2597−2605.

[13] DU Jun, YANG Jian, KUWABARA M, LI Wen-fang, PENG Ji-hua. Effect of strontium on the grain refining efficiency of Mg−3Al alloy refined by carbon inoculation [J]. Journal of Alloys and Compounds, 2009, 470: 228−232.

[14] LI Cheng-bo, YANG Shu-qing, DU Jun, LIAO Heng-bin, LUO Gan. Synergistic refining mechanism of Mg−3%Al alloy refining by carbon inoculation combining with Ca addition [J]. Journal of Magnesium and Alloys, 2020, 8: 1090−1101.

[15] WEI Jie, WANG Qu-dong, ZHANG Li, YIN Dong-di, YE Bing, JIANG Hai-yan, DING Wen-jiang. Microstructure refinement of Mg−Al−RE alloy by Gd addition [J]. Materials Letters, 2019, 246: 125−128.

[16] WANG Cun-long, DAI Ji-chun, LIU Wen-cai, ZHANG Liang, WU Guo-hua. Effect of Al additions on grain refinement and mechanical properties of Mg−Sm alloys [J]. Journal of Alloys and Compounds, 2015, 620: 172−179.

[17] QIU Dong, ZHANG Ming-xing. The nucleation crystallography and wettability of Mg grains on active Al_2Y inoculants in an Mg−10wt.%Y alloy [J]. Journal of Alloys and Compounds, 2014, 586: 39−44.

[18] CHANG H W, QIU D, TAYLOR J A, EASTON M A, ZHANG M X. The role of Al_2Y in grain refinement in Mg−Al−Y alloy system [J]. Journal of Magnesium and Alloys, 2013, 1: 115−121.

[19] LIAO Heng-bin, ZHAN Mei-yan, LI Cheng-bo, MA Zhi-qiang, DU Jun. Grain refinement of Mg−Al alloys inoculated by $MgAl_2O_4$ powder [J]. Journal of Magnesium and Alloys, 2021, 9: 1211−1219.

[20] MA Zhi-qiang, LI Cheng-bo, DU Jun, ZHAN Mei-yan. Grain refinement of Mg−Al alloys inoculated by MgO powder [J]. International Journal of Metalcasting, 2019, 13: 674−685.

[21] PENG G S, WANG Y, FAN Z. Competitive heterogeneous nucleation between Zr and MgO particles in commercial purity magnesium [J]. Metallurgical and Materials Transactions A, 2018, 49: 2182−2192.

[22] ALI Y, QIU Dong, JIANG Bin, PAN Fu-sheng, ZHANG Ming-xing. The influence of CaO addition on grain refinement of cast magnesium alloys [J]. Scripta Materialia, 2016, 114: 103−107.

[23] LIU Xuan, ZHANG Zhi-qiang, LE Qi-chi, BAO Lei. The effects of ZnO particles on the grain refinement and mechanical properties of AZ31 magnesium alloys [J]. Transactions of the Indian Institute of Metals, 2016, 69: 1911−1918.

[24] TAAMTZIS S, ZHANG H, BABU N H, FAN Z. Microstructural refinement of AZ91D die-cast alloy by intensive shearing [J]. Materials Science and Engineering: A, 2010, 527: 2929−2934.

[25] FAN Z, WANG Y, XIA M, ARUMUGANATHAR S. Enhanced heterogeneous nucleation in AZ91D alloy by intensive melt shearing [J]. Acta Materialia, 2009, 57: 4891−4901.

[26] YANG Shu-qing, LI Cheng-bo, LUO Gan, DU Jun, ZHAO Yu-jun. Mg adsorption on $MgAl_2O_4$ surfaces and the effect of additive Ca: A combined experimental and theoretical study [J]. Journal of Alloys and Compounds, 2021, 861: 158564.

[27] FU H M, QIU D, ZHANG M X, WANG H, KELLY P M, TAYLOR J A. The development of a new grain refiner for magnesium alloys using the edge-to-edge model [J]. Journal of Alloys and Compounds, 2008, 456: 390−394.

[28] HARINI R S, RAJ B, RAVI K R. Synthesis of Al−$MgAl_2O_4$ master alloy and its grain refinement studies in pure aluminium [J]. Transactions of the Indian Institute of Metals, 2015, 68: 1059−1063.

[29] HARINI R S, NAMPOOTHIRI J, NAGASIVAMUNI B, RAJ B, RAVI K R. Ultrasonic assisted grain refinement of Al−Mg alloy using in-situ $MgAl_2O_4$ particles [J]. Materials Letters, 2015, 145: 328−331.

[30] LI H T, WANG Y, FAN Z. Mechanisms of enhanced heterogeneous nucleation during solidification in binary Al−Mg alloys [J]. Acta Materialia, 2012, 60: 1528−1537.

[31] SHIH T S, LIU J B, WEI P S. Oxide films on magnesium and magnesium alloys [J]. Materials Chemistry and Physics, 2007, 104: 497−504.

[32] SHIH T S, WANG J H, CHONG K Z. Combustion of magnesium alloys in air [J]. Materials Chemistry and Physics, 2004, 85: 302−309.

[33] TONG Xin, YOU Guo-qiang, LIU Yan, LONG Si-yuan, LIU Qing. Effect of C_2H_2 as a novel gas inoculant on the microstructure and mechanical properties of as-cast AM60B magnesium alloy [J]. Journal of Materials Processing Technology, 2019, 271: 271−283.

[34] PARK J H. Effect of inclusions on the solidification structures of ferritic stainless steel: Computational and experimental study of inclusion evolution [J]. Calphad, 2011, 35: 455−462.

[35] MIZOGUCHI S, TAKAMURA J. Control of oxides as inoculants metallurgy of oxides in steel process [C]//Sixth International Iron and Steel Congress. Nagoya, ISIJ, 1990: 2331−2342.

[36] LIAO Heng-bin, MO Li-ling, ZHOU Xiong, ZHAO Bin, DU Jun. Grain refinement and improvement of mechanical properties of AZ31 magnesium alloy inoculated by in-situ oxidation process [J]. Journal of Materials Research and Technology, 2021, 12: 807−817.

[37] SONG Hong-quan, ZHAO Ming, LI Jian-guo. First-principles study of Mg(0001)/MgO($1\bar{1}$1) interfaces [J]. Modern Physics Letters, 2016, 30: 1650152.

[38] LIU Zhi-lin. Review of grain refinement of cast metals through inoculation: Theories and developments [J]. Metallurgical and Materials Transactions A, 2017, 48:

4755−4776.
[39] Lawrence Berkeley National Laboratory. Materials project [EB/OL]. 2021−04−12. Https://materialsproject.org/#search/thermo.
[40] CAMPBELL J. Castings [M]. 2nd ed. Oxford: Elsevier, 2004.
[41] GREER A L, BUNN A M, TRONCHE A, EVANS P V, BRISTOW D J. Modelling of inoculation of metallic melts: Application to grain refinement of aluminium by Al−Ti−B [J]. Acta Materialia, 2000, 48: 2823−2835.
[42] STJOHN D H, QIAN M, EASTON M A, CAO P. The interdependence theory: The relationship between grain formation and nucleant selection [J]. Acta Materialia, 2011, 59: 4907−4921.

Mg−Al 二元合金原位氧化孕育细化

廖恒斌[1]，莫丽玲[1]，李乘波[1,2]，詹美燕[1]，杜 军[1]

1. 华南理工大学 材料科学与工程学院，广州 510640；
2. 广西民族大学 材料与环境学院，南宁 530006

摘 要：利用氧化夹杂诱发异质形核是实现晶粒细化的有效途径。本研究通过原位氧化工艺实现 Mg−Al 二元合金的晶粒细化。结果表明，MgO 和 $MgAl_2O_4$ 是原位氧化孕育 Mg−*x*Al 合金的主要氧化产物。对于纯 Mg 和 Mg−1Al 合金，MgO 是唯一的氧化产物。当 Mg−*x*Al 合金中 Al 含量增加到 3%(质量分数)时，$MgAl_2O_4$ 是另一种氧化产物。经过原位氧化孕育，Mg−3Al 合金的平均晶粒尺寸由 1135 μm 显著减小至 237 μm，晶粒细化率高达 79.1%。MgO 和 $MgAl_2O_4$ 都具有形核 *α*-Mg 晶粒的能力。$MgAl_2O_4$ 与 *α*-Mg 的错配度更小，表现出更高的形核能力。原位氧化工艺孕育细化 Mg−*x*Al 合金归因于 *α*-Mg 晶粒在 MgO 或 $MgAl_2O_4$ 颗粒上的异质形核。

关键词：Mg−Al 合金；晶粒细化；异质形核；MgO；$MgAl_2O_4$

(Edited by Wei-ping CHEN)